Finite element periodic catenary model to perform HIL pantograph tests considering non-linear dropper behaviour

J. Gil[a], M. Tur[a], S. Gregori[a,*], A. Correcher[b], F.J. Fuenmayor[a]

[a]*Instituto de Ingeniería Mecánica y Biomecánica, Universitat Politècnica de València,*
Camino de Vera s/n, 46022, Valencia (Spain)
[b]*Instituto de Automática e Informática Industrial, Universitat Politècnica de València,*
Camino de Vera s/n, 46022, Valencia (Spain)

Abstract

In this paper, we propose a general approach to compute the dynamic response of periodic infinite structures subjected to a moving load. The method only considers one repetitive block of the structure which is modelled by the Finite Element Method. The problem is first shifted to the frequency domain where the periodicity condition is easily applied and then the temporal response is obtained. An infinite periodic catenary system has been chosen to illustrate the proposed formulation. The linear formulation is extended to include the non-linear behaviour of droppers. The efficiency and accuracy of the catenary model obtained makes it very suitable for use in Hardware in the Loop (HIL) pantograph tests. We propose to combine this catenary model with an iterative strategy to achieve the steady-state response of the coupled system and its performance is analysed in a virtual HIL simulation.

Keywords: Non-linear periodic structures, Moving load, Pantograph-catenary interaction, Hardware-in-the-loop, Finite Element Method

---

*Corresponding author

1. Introduction

1.1. Background

In the last decades, the expansion of electric railway systems has brought an important increase in the number of investigations focused on pantograph-catenary dynamic interaction. The proper sliding contact between both systems is crucial to achieve higher velocities, to reduce the wear of the sliding interfaces and to ensure a stable and safety operation. The pantograph is a mechanism that is mounted on the roof of the locomotive, which keeps contact with the contact wire of the catenary by pushing it up. This interaction has been studied by means of different techniques as it is described in [1]. Essentially, the three main options are: numerical simulations, hardware-in-the-loop (HIL) tests or hybrid simulations and in-line testing.

Numerical simulations are widely used being the Finite Element Method (FEM) the most chosen approach. A deep analysis of the results of a pantograph-catenary interaction benchmark can be found in [2] and the references therein, which included the participation of 10 international research groups. Hybrid simulations or HIL tests are in the midway between numerical simulations and in-line testing. They consist on splitting the whole system into two substructures, being one of them replaced by a numerical model while the other is physically present in the simulation. The interaction between both systems, namely the virtual and the physical, is carried out by an interface made up by sensors and actuators. An insightful review of hybrid simulations applied to different systems can be found in [3]. This approach has also been applied successfully to the pantograph-catenary system [4]. In this case, the pantograph is the physical substructure and the catenary is replaced by a numerical model playing the role of the virtual system.

1.2. Problem of interest

The implementation of HIL pantograph tests involves certain issues and challenges. The catenary model must be solved in real time while keeping a

2

high accuracy and there is usually a control-loop delay between the contact force measurement time and the imposition to the pantograph collector of the displacement computed from the catenary model. In order to solve these issues, some authors proposed different degrees of simplification in the catenary model used that compromise the accuracy of the results obtained. This work is aimed at setting an entire framework that allows HIL testing with a high accuracy in the catenary model.

As depicted in Fig. 1, a catenary section is composed of a succession of spans. In its central region they use to be equal, which leads to a repetitive structure that presents a steady-state response when interacting with the pantograph. We choose the FEM to model the catenary and we assume the hypothesis of periodicity that is representative of the most part of the catenary. Furthermore, to achieve realistic results, the non-linear behaviour of droppers must be considered, which is also a challenge dealt with in this work.

However, if we consider a steady-state response it can present some disadvantages such as the inability to consider uneven spans, realistic contact wire irregularities and overlaps between consecutive sections. The influence of these phenomena was studied in [5, 6], concluding that their effect is not the most significant on the overall catenary dynamic response.

The procedure to implement a HIL test with a periodic catenary model includes two clearly differentiated parts. The first stage consists on creating a periodic catenary FEM model which reproduces the steady-state regime subject to a constant velocity moving load. In the formulation proposed in this work, only one span is discretised by the FEM and periodic boundary conditions are applied on the ends of the model to avoid modelling the entire catenary. The second stage is focused on defining a methodology to use the proposed periodic model, which represents the steady-state response of the catenary, in a HIL pantograph test, which unavoidably presents control-loop delays and an initial transient regime.

3
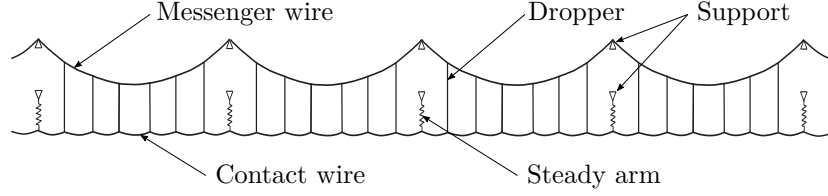
Figure 1: *Main components of a railway catenary.*

1.3. Literature review

In this subsection we present a literature review of the problem addressed in this work, distinguishing the works related to periodic models subjected to moving loads and the works that deal with HIL pantograph tests.

A broad overview of the dynamic response of structures under moving loads can be found in [7], in which the solution of different moving-load problems are discussed from an analytical point of view. The study of this type of prob-lems has gained interest in the analysis of the steady-state response of systems such as rails, overhead contact lines or bridges. This problem has been tra-ditionally addressed with analytic models based on a periodically supported infinite string/ beam [8–10]. These approaches have in common the considera-tion of a periodic solution which allows considering only a repetitive block of the model between two consecutive supports. Specifically, an infinite periodic Euler-Bernoulli beam subjected to a uniform moving harmonic pressure field is used in [8] to simulate the dynamic behaviour of the rail. The differential equation is solved in the domain defined between two supports to which appro-priate boundary periodicity conditions are applied. A similar model is proposed in [9], in which a modal representation results in a system of uncoupled differ-ential equations. The limit of the solution of such a system when the number of blocks tends to infinity is computed for a moving constant load. The same problem is also solved in [10], applying the Fourier Transform to shift to the frequency domain where the periodicity condition is more easily formulated. The solution in the frequency domain is moved back to the time domain by the Inverse Fourier Transform.

4

The main limitation to the previous solutions is the simplicity of the model used, with which it is not possible to model more complex structures. To this end, some solutions are proposed in the literature. An extension of the approach given in [10] is presented in [11] to solve a catenary model that includes two interconnected strings. Two-and-a-half dimensional (2.5D) Finite Element models appear as an alternative to solve infinite periodic structures with constant cross section. This strategy is applied in [12], to model a rail. Fourier Transform with respect to space and time is performed to solve the problem which allows the application of the periodicity condition on the reactions of the supports in the frequency domain. The same authors presented an improved model in [13] where the dynamic interaction of multiple wheels with the periodic model is computed by means of Fourier series decomposition of the contact force.

A more general method is the so-called Wave Finite Element Method (WFEM) that is not only used to model infinite periodic structures, but also can be ap-plied to finite periodic structures [14, 15]. WFEM is used in [16] to obtain the frequency response function of a periodic infinite structure which is used to compute the response of the system excited by a moving load. WFEM also allows to consider structures with transition zones [15].

Regarding the HIL tests applied to the pantograph-catenary interaction, it can be found in the literature several solutions that include different degrees of simplification to carry out the tests. The first works that presented a pantograph HIL test rig were [17, 18]. They used a finite length linear catenary model based on a truncated modal approach. Another HIL set-up was proposed in [19] with a simple catenary model composed of three spans and a sliding window strategy. This model was upgraded in [20] with the consideration of dropper slackening and in [21], with the incorporation of lateral movement to the test rig to simulate the catenary stagger. A linear catenary model is used in [22] for HIL tests using 3D Euler-Bernoulli beams discretised with finite differences based on a moving coordinate formulation in combination with an absorbing boundary layer to attenuate outgoing waves. Other appealing catenary model intended to perform HIL pantograph tests was proposed in [23]. It is based on a modal truncation

5

of a full FE model, which would allow to consider non-periodic features such as overlaps or installations errors. However, the practical use of this model in HIL tests is challenging due to the presence of control-loop delays that can make the test unstable.

1.4. Scope and contributions of this study

This paper is aimed at: i) solving the steady-state interaction of constant velocity moving loads with periodic structures modelled by the FEM and ii) proposing an strategy to use that solution to perform HIL tests. The global objective is to define a complete framework to perform high fidelity HIL pantograph tests dealing with the usual control-loop delay that appears in this type of tests.

The Periodic Finite Element Model (PFEM) of the catenary proposed accomplishes the first aim of this work and overcomes some of the limitations of other models found in the literature. The PFEM allows modelling more complex structures than the analytical models [8–10, 10], multi-strings models [10, 11] and 2.5D FEM models [12, 13]. Furthermore, it is a general method that can be applied to any periodic structure modelled by the FEM. WFEM [14, 15] can provide a similar solution by means of the method proposed in [16], however, when WFEM is applied to slender structures with long spatial period such as a railway catenary, some numerical problems arise making its solution not usable in practise. Additionally, control-loop delays can be easily handled with the catenary PFEM unlike with full FE catenary models, in which the response of the catenary in future steps is not known in advance.

The final proposed model results very suitable for its application in HIL tests and provides more accurate results than other catenary models used for this purpose. In [17, 18], the accuracy of the model is limited due to either the severe modal truncation considered or the small length of the system modelled to fulfil both memory requirements and real-time performance. Sliding window methods [19–21] also focus on the steady-state response but the boundary con-ditions imposed lead to not negligible errors. Even in [22], in which boundary

6

layers are used to avoid undesirable effects on the ends of the model, the fidelity of the results is compromised. The model proposed in this paper avoids these boundary effects by considering periodic boundary conditions that lead to the proper steady-state response. Additionally, it has the potential to compensate the control-loop delay that appears in HIL tests. Unlike most models found in the literature, other important contribution of this work relies on considering the non-linear behaviour of droppers, which are not able to hold compressive forces. This feature is essential to obtain high-fidelity results in HIL pantograph tests.

The second aim of this work is accomplished by adapting the iterative procedure proposed in [24] to the scenario of a periodic catenary model. This procedure allows both the virtual catenary and the physical pantograph to achieve the steady-state regime in a HIL test.

1.5. Organisation of the paper

The paper is structured as follows. The case of study of this work is described in Section 2. In Section 3, the impulse response of the catenary FE model with periodicity conditions is computed by solving the problem in the frequency domain. This impulse response is used in Section 4 combined with an iterative procedure to perform HIL pantograph tests. The model is enhanced in Section 5 to include the non-linear behaviour of droppers and some numerical results to verify the computational costs and the accuracy of the proposed model are presented in Section 6. A discussion and the main concluding remarks are given in Section 7. Finally, a demonstrative example that facilitates the reproduction of some numerical results is included in Appendix A.

2. Description of the case study

The formulation developed in this paper is general in the sense that it can be applied to any periodic structure as long as it can be modelled by the FEM. However, as the final goal of this study is to perform HIL pantograph tests, the proposed formulation is applied to a railway catenary model along the paper.

As depicted in Fig. 1, a catenary is mainly composed of a contact wire, which interacts with the pantograph and is held by the messenger wire through verti-cal cables called droppers. The wiring is supported at regular intervals defining a span between two consecutive supports. The parameters that define the cate-nary and the pantograph models which are used to obtain the results presented in Section 6 can be found in [2]. Additionally, the pantograph-catenary dy-namic interaction is solved according to the method proposed in [25] when full FE simulations are required for comparison and validation purposes.

To obtain the PFEM proposed in this work it is only necessary to obtain the FE model of the repeated block of the structure, in this case one span of the catenary, to apply the formulation described in the following sections. The resulting catenary PFEM is suitable to perform HIL pantograph tests in which the contact force applied to the pantograph collectors is measured and the displacement of the contact point obtained from the catenary PFEM is imposed by means of an actuator. In this work, all the HIL environment is treated by means of simulations, leaving for future work the application to real HIL tests. To this end, the physical substructure (i.e. the pantograph) is also simulated with a numerical model to evaluate the capabilities of the proposed method.

3. Impulse response of the catenary

In this section, we present a general method to obtain the impulse response of an infinite periodic structure subject to a periodic load moving at constant speed. To illustrate the method, a railway catenary has been chosen as shown in Fig. 2. As a periodic structure, the catenary is subdivided into consecutive blocks b of length L, which are repeated infinitely in the longitudinal direction $\mathbf{e}_1$. A 2D catenary is depicted in Fig. 2 in which each periodic block b is a single span. In the case of a 3D catenary, the repetitive block would consist of two spans, due to the stagger arrangement of the catenary wires. It is important to note that, as opposed to applying moving window strategies, the accuracy of the proposed method is not further improved by including more spans into the
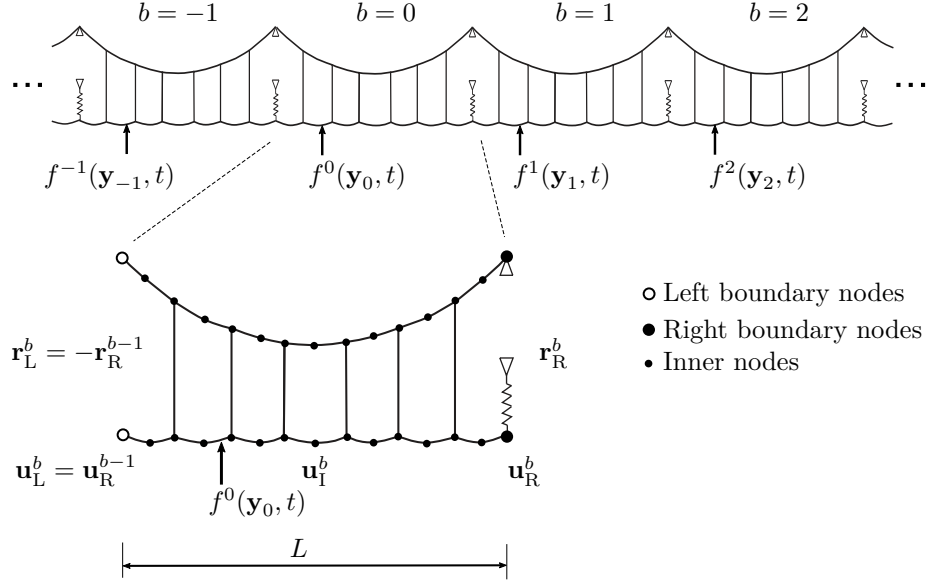
Figure 2: *Catenary as a periodic infinite structure and Finite Element discretization of block $b = 0$.*

repetitive block.

The pantograph moves at a constant speed V and the interaction with the catenary will be indefinitely repeated at every block if one considers that the stationary state is achieved. Therefore, the external contact force applied to the catenary is a periodic moving load of period $T = L/V$.

Under the hypothesis of periodic interaction, any force applied in a given block b is actually applied sequentially in every block $b \in [-\infty, \infty]$ at the same instant with respect to that in which the pantograph started to interact with each block. It is possible to calculate the impulse response produced by a sequence of unit impulses $f^b(\mathbf{y}_b, t)$, which are periodically applied in each block b (only once per block) at points $\mathbf{y}_b$ and at time $t = bT$, as depicted in Fig. 2.

The sequence of unit impulses that defines the impulse response can be defined as:

$$f^b(\mathbf{y}_b, t) = \delta(t - bT) \qquad b = -\infty, \ldots, \infty \tag{1}$$

in which δ is the Dirac function and they are applied to every block b at the

9

global coordinate $\mathbf{y}_b = \mathbf{y} + bL\mathbf{e}_1$.

Given a point $\mathbf{y}$ in the reference block $b = 0$, the sequence of infinite unit impulses $f^b(\mathbf{y}, t)$ produces the catenary displacement $u(t, \mathbf{x}, \mathbf{y})$ at point $\mathbf{x}$. In this case, this is the unit impulse response $h(t, \mathbf{x}, \mathbf{y})$ under periodic con-
220   ditions. Note that the coordinates of the excitation point are denoted by vector $\mathbf{y} = [y_1, y_2, y_3]^\top$ whereas, the coordinates of the point at which the response is measured are referred to as $\mathbf{x} = [x_1, x_2, x_3]^\top$. Both the impulse excitation f^b and catenary displacement u can be defined in an arbitrary direction, which are not explicitly indicated for simplification in the notation.

225   The stationary response of the catenary u, will be repeated in each block. Thus, for a given point $\mathbf{x}$, the periodicity condition reads as:

$$u(t, \mathbf{x}, \mathbf{y}) = u(t - bT, \mathbf{x} + bL\mathbf{e}_1, \mathbf{y}) \tag{2}$$

which allows the description of the response of the entire catenary with that of a single block, so that the response of the reference block $b = 0$ will be considered herein after. If this reference block is discretised by the Finite Element Method
230   (FEM), the displacements of its N_{dof} nodal degrees of freedom are denoted by $\mathbf{u}^0(t, \mathbf{y})$ or $\mathbf{u}(t, \mathbf{y})$ in which superscript 0 is deleted for simplicity in the notation. The nodes of the FE mesh of the reference block can be divided into left (L) and right (R) boundary nodes and inner (I) nodes as shown in Fig. 2.

3.1. Frequency Response Function

235   The impulse response of the above described infinite periodic system will be obtained by considering only the reference block [8–10] and imposing the periodicity condition defined in Eq. (2). Some authors have solved this problem by applying the Floquet decomposition [26]. However, we followed the strategy proposed in [10, 11], which is based on the movement of the problem to the
240   frequency domain in which the periodicity condition is more easily stated. Thus, we first need to find the Frequency Response Function (FRF) that relates the displacement of point $\mathbf{x}$ to a harmonic unit force of frequency ω applied at point $\mathbf{y}$.

10

Without loss of generality, in this work, the displacements of inner and right boundary nodes, $\mathbf{u}_\mathrm{I}(t)$ and $\mathbf{u}_\mathrm{R}(t)$ respectively, are chosen as the unknowns of the problem. Displacements of the left boundary nodes $\mathbf{u}_\mathrm{L}$ must fulfil Eq. (2), that is:

$$\mathbf{u}_\mathrm{L}(t) = \mathbf{u}_\mathrm{R}(t+T) \tag{3}$$

which after applying the Fourier Transform, it becomes:

$$\mathbf{U}_\mathrm{L}(\omega) = e^{i\omega T}\mathbf{U}_\mathrm{R}(\omega) \tag{4}$$

being $\mathbf{U}_\mathrm{L,I,R}(\omega)$ the Fourier Transform of $\mathbf{u}_\mathrm{L,I,R}(t)$, respectively.

The nodal equivalent external force vector $\mathbf{F}$ can be divided into left, inner and right nodal degrees of freedom, namely $\mathbf{F}_\mathrm{L}$, $\mathbf{F}_\mathrm{I}$ and $\mathbf{F}_\mathrm{R}$, respectively. If the degrees of freedom of left and right boundary nodes are properly defined (mesh compatibility), $\mathbf{F}_\mathrm{L}$ and $\mathbf{F}_\mathrm{R}$ are related through the following equation:

$$\mathbf{F}_\mathrm{L} = e^{i\omega T}\mathbf{F}_\mathrm{R} \tag{5}$$

The FRF of the system can be found by solving the following problem for every frequency:

$$\mathbf{D}(\omega)\,\mathbf{U} = \mathbf{F} + \mathbf{R}$$
$$\mathbf{D}(\omega) = \mathbf{K} + i\omega\mathbf{C} - \omega^2\mathbf{M} \tag{6}$$

where $\mathbf{M}$ is the mass matrix, $\mathbf{K}$ the stiffness matrix and $\mathbf{C}$ the damping matrix of the substructure contained in a single block. The reaction force vector $\mathbf{R}$, applied to the left and right boundary nodes $\mathbf{R} = [\mathbf{R}_\mathrm{L},\ \mathbf{0},\ \mathbf{R}_\mathrm{R}]^\top$, is also unknown. Eq. (6) can be rearranged in left boundary, inner and right boundary degrees of freedom:

$$\begin{bmatrix} \mathbf{D}_\mathrm{LL} & \mathbf{D}_\mathrm{LI} & \mathbf{D}_\mathrm{LR} \\ \mathbf{D}_\mathrm{IL} & \mathbf{D}_\mathrm{II} & \mathbf{D}_\mathrm{IR} \\ \mathbf{D}_\mathrm{RL} & \mathbf{D}_\mathrm{RI} & \mathbf{D}_\mathrm{RR} \end{bmatrix} \left\{ \begin{array}{c} \mathbf{U}_\mathrm{L} \\ \mathbf{U}_\mathrm{I} \\ \mathbf{U}_\mathrm{R} \end{array} \right\} = \left\{ \begin{array}{c} \mathbf{F}_\mathrm{L} \\ \mathbf{F}_\mathrm{I} \\ \mathbf{F}_\mathrm{R} \end{array} \right\} + \left\{ \begin{array}{c} \mathbf{R}_\mathrm{L} \\ \mathbf{0} \\ \mathbf{R}_\mathrm{R} \end{array} \right\} \tag{7}$$

Considering again the periodicity condition and the action reaction principle, the reaction force vector in the left and right boundary $\mathbf{R}_\mathrm{L}$ and $\mathbf{R}_\mathrm{R}$ are related

11

by:

$$\mathbf{R}_{\mathrm{L}} = -e^{i\omega T}\mathbf{R}_{\mathrm{R}} \tag{8}$$

Introducing Eqs. (4) and (5) to Eq. (7):

$$
\begin{bmatrix}
\mathbf{D}_{\mathrm{LI}} & \mathbf{D}_{\mathrm{LR}} + e^{i\omega T}\mathbf{D}_{\mathrm{LL}} \\
\mathbf{D}_{\mathrm{II}} & \mathbf{D}_{\mathrm{IR}} + e^{i\omega T}\mathbf{D}_{\mathrm{IL}} \\
\mathbf{D}_{\mathrm{RI}} & \mathbf{D}_{\mathrm{RR}} + e^{i\omega T}\mathbf{D}_{\mathrm{RL}}
\end{bmatrix}
\left\{
\begin{array}{c}
\mathbf{U}_{\mathrm{I}} \\
\mathbf{U}_{\mathrm{R}}
\end{array}
\right\}
=
\left\{
\begin{array}{c}
e^{i\omega T}\mathbf{F}_{\mathrm{R}} \\
\mathbf{F}_{\mathrm{I}} \\
\mathbf{F}_{\mathrm{R}}
\end{array}
\right\}
+
\left\{
\begin{array}{c}
\mathbf{R}_{\mathrm{L}} \\
\mathbf{0} \\
\mathbf{R}_{\mathrm{R}}
\end{array}
\right\}
\tag{9}
$$

265 and then using Eq. (8), the unknowns can be rearranged to the left-hand side:

$$
\begin{bmatrix}
\mathbf{D}_{\mathrm{LI}} & \mathbf{D}_{\mathrm{LR}} + e^{i\omega T}\mathbf{D}_{\mathrm{LL}} & e^{i\omega T}\mathbf{I} \\
\mathbf{D}_{\mathrm{II}} & \mathbf{D}_{\mathrm{IR}} + e^{i\omega T}\mathbf{D}_{\mathrm{IL}} & \mathbf{0} \\
\mathbf{D}_{\mathrm{RI}} & \mathbf{D}_{\mathrm{RR}} + e^{i\omega T}\mathbf{D}_{\mathrm{RL}} & -\mathbf{I}
\end{bmatrix}
\left\{
\begin{array}{c}
\mathbf{U}_{\mathrm{I}} \\
\mathbf{U}_{\mathrm{R}} \\
\mathbf{R}_{\mathrm{R}}
\end{array}
\right\}
=
\begin{bmatrix}
\mathbf{0} & e^{i\omega T}\mathbf{I} \\
\mathbf{I} & \mathbf{0} \\
\mathbf{0} & \mathbf{I}
\end{bmatrix}
\left\{
\begin{array}{c}
\mathbf{F}_{\mathrm{I}} \\
\mathbf{F}_{\mathrm{R}}
\end{array}
\right\}
\tag{10}
$$

in which $\mathbf{I}$ denotes for the identity matrix. Problem (10) can be solved as:

$$
\left\{
\begin{array}{c}
\mathbf{U}_{\mathrm{I}} \\
\mathbf{U}_{\mathrm{R}} \\
\mathbf{R}_{\mathrm{R}}
\end{array}
\right\}
= \hat{\mathbf{H}}(\omega)
\left\{
\begin{array}{c}
\mathbf{F}_{\mathrm{I}} \\
\mathbf{F}_{\mathrm{R}}
\end{array}
\right\}
\tag{11}
$$

where:

$$
\hat{\mathbf{H}}(\omega) =
\begin{bmatrix}
\mathbf{D}_{\mathrm{LI}} & \mathbf{D}_{\mathrm{LR}} + e^{i\omega T}\mathbf{D}_{\mathrm{LL}} & e^{i\omega T}\mathbf{I} \\
\mathbf{D}_{\mathrm{II}} & \mathbf{D}_{\mathrm{IR}} + e^{i\omega T}\mathbf{D}_{\mathrm{IL}} & \mathbf{0} \\
\mathbf{D}_{\mathrm{RI}} & \mathbf{D}_{\mathrm{RR}} + e^{i\omega T}\mathbf{D}_{\mathrm{RL}} & -\mathbf{I}
\end{bmatrix}^{-1}
\begin{bmatrix}
\mathbf{0} & e^{i\omega T}\mathbf{I} \\
\mathbf{I} & \mathbf{0} \\
\mathbf{0} & \mathbf{I}
\end{bmatrix}
\tag{12}
$$

Eq. (11) can be rewritten in terms of the displacements of the block as:

$$
\left\{
\begin{array}{c}
\mathbf{U}_{\mathrm{L}} \\
\mathbf{U}_{\mathrm{I}} \\
\mathbf{U}_{\mathrm{R}}
\end{array}
\right\}
= \mathbf{H}(\omega)
\left\{
\begin{array}{c}
\mathbf{F}_{\mathrm{I}} \\
\mathbf{F}_{\mathrm{R}}
\end{array}
\right\}
\tag{13}
$$

with

$$
\mathbf{H}(\omega) =
\begin{bmatrix}
e^{i\omega T}\hat{\mathbf{H}}_{\mathrm{R}}(\omega) \\
\hat{\mathbf{H}}_{\mathrm{I}}(\omega) \\
\hat{\mathbf{H}}_{\mathrm{R}}(\omega)
\end{bmatrix}
\tag{14}
$$

270 in which $\hat{\mathbf{H}}_{\mathrm{I}}(\omega)$ and $\hat{\mathbf{H}}_{\mathrm{R}}(\omega)$ are the two first rows of $\hat{\mathbf{H}}(\omega)$.

12

3.2. Impulse response

Eq. (13) relates nodal displacements with nodal forces of the entire block by means of the FRF $\mathbf{H}(\omega)$. However, we are interested in the displacement of point $\mathbf{x}$ produced by a unit harmonic force F_u applied at point $\mathbf{y}$ in the reference block. The FEM operator $\mathbf{N}(\mathbf{x}) = [\mathbf{N}_{\mathrm{L}}(\mathbf{x}), \ \mathbf{N}_{\mathrm{I}}(\mathbf{x}), \ \mathbf{N}_{\mathrm{R}}(\mathbf{x})]$ is the $1 \times N_{\mathrm{dof}}$ matrix, composed of nodal shape functions that transforms nodal displacements into point displacements in a given direction and can also be used to transform point forces to nodal equivalent forces.

With this operator, the nodal equivalent forces relative to the unit force F_{u} can be written as:

$$\left\{ \begin{array}{c} \mathbf{F}_{\mathrm{I}} \\ \mathbf{F}_{\mathrm{R}} \end{array} \right\} = \left\{ \begin{array}{c} \mathbf{N}_{\mathrm{I}}(\mathbf{y})^\top \\ \mathbf{N}_{\mathrm{R}}(\mathbf{y})^\top + e^{-i\omega T}\mathbf{N}_{\mathrm{L}}(\mathbf{y})^\top \end{array} \right\} \tag{15}$$

in which the term $e^{-i\omega T}\mathbf{N}_{\mathrm{L}}(\mathbf{y})^\top$ considers the nodal forces at the right boundary of the reference block ($b = 0$) that would appear if the unit force was applied on the next block ($b = 1$). Note that this contribution is only active if the unit force is applied on an element of the reference block that has some node on the left boundary.

With the use of the operator $\mathbf{N}(\mathbf{x})$ applied to the right-hand side of Eq. (13) and including Eq. (15), it is possible to compute the harmonic displacement of point $\mathbf{x}$ when a unit harmonic force acts at $\mathbf{y}$:

$$I(\omega, \mathbf{x}, \mathbf{y}) = \mathbf{N}(\mathbf{x})\, \mathbf{H}(\omega) \left\{ \begin{array}{c} \mathbf{N}_{\mathrm{I}}(\mathbf{y})^\top \\ \mathbf{N}_{\mathrm{R}}(\mathbf{y})^\top + e^{-i\omega T}\mathbf{N}_{\mathrm{L}}(\mathbf{y})^\top \end{array} \right\} \tag{16}$$

As the structure is modelled with FEM, Eq. (16) cannot be analytically defined but is computed for a discrete number of frequencies N_{f} with a frequency increment $\Delta\omega$:

$$\omega_k = k\Delta\omega \qquad k = 0, \ldots, N_{\mathrm{f}} - 1 \tag{17}$$

In addition, time t is also discretised with a time increment Δt:

$$t_n = n\Delta t \tag{18}$$

13

Thus, applying the Inverse Discrete Fourier Transform to Eq. (16), the impulse response at time step t_n is obtained as:

$$h(t_n, \mathbf{x}, \mathbf{y}) = \sum_{k=0}^{N_f-1} a_k \mathrm{Re}\left(I(\omega_k, \mathbf{x}, \mathbf{y})\, e^{i\omega_k n \Delta t}\right) \Delta\omega \qquad (19)$$

being $a_k = 2$ if $k \neq 0$ or $a_k = 1$ if $k = 0$.

It is important to remark that there is no relation between $\Delta\omega$ and the period T. In practise, $\Delta\omega$ has to be chosen little enough to obtain an accurate time response and N_f is limited by Δt to avoid aliasing effects.

4. Hardware In the Loop test methodology with a linear catenary model

The concept of Hardware In the Loop (HIL) tests applied to railway pantographs consists of hybrid simulations with a virtual catenary model and a physical pantograph (see Fig. 3). In these tests, the catenary is replaced by an actuator that interacts with a real pantograph and simulates the vertical movement of the catenary contact point. The contact force measured in the test rig is the input of the virtual catenary model which must supply the contact point vertical position in real time.
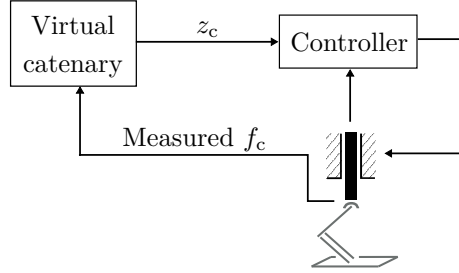

Figure 3: *Scheme of a HIL pantograph test.*

Eq. (19) condenses the linear behaviour of the periodic catenary under a moving periodic load, so that non-linear effects such as dropper slackening are not considered in this section. Thus, the general response can be obtained with the load applied at the contact wire of a single block.

14

The pantograph is virtually moving at a constant speed V and applies a vertical excitation over the contact wire of the catenary model. Δt is chosen so that the contact wire of a periodic block of length L is divided in N_c virtual contact points $\mathbf{y}_{cw}(t_n)$ with $n = 0, \ldots, N_c - 1$.
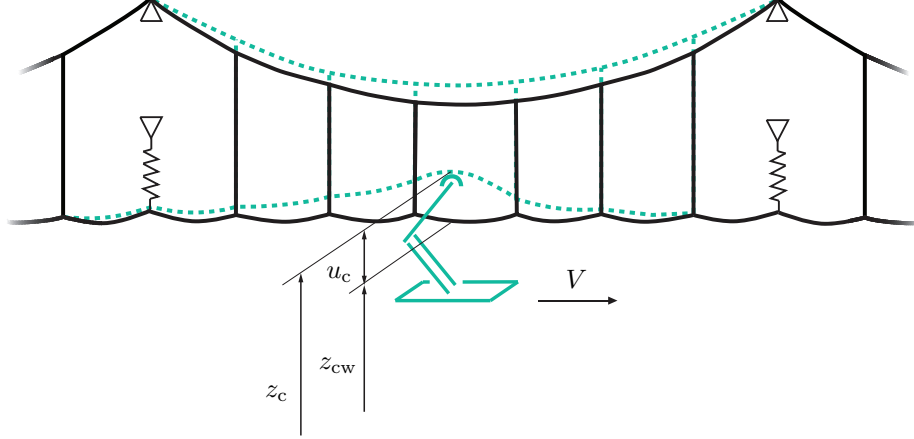
Figure 4: *Pantograph interaction with the periodic catenary.*

If the contact force $f_c(t_n)$ applied to a virtual contact point $\mathbf{y}_{cw}(t_n)$ is assumed to be known, Eq. (19) can be particularised to compute the vertical displacement $u(t_n, \mathbf{x})$ of a given point $\mathbf{x}$, by applying the superposition principle as the sum of the contribution of each force applied on the block:

$$u(t_n, \mathbf{x}) = \sum_{\hat{n}=0}^{N_c-1} h(t_n - t_{\hat{n}}, \mathbf{x}, \mathbf{y}_{cw}(t_{\hat{n}}))\, f_c(t_{\hat{n}})\Delta t \qquad (20)$$

Note that $\hat{n}$ denotes the time instant at which the force is applied and n, the instant at which the displacement is evaluated. It should also be noted that the origin of time in the impulse response function (Eq. (19)) corresponds to the instant at which the impulse is applied. However, in Eq. (20), $t_n = 0$ which is the time step at which the force is applied at the beginning of the block. This is the reason why the impulse function is evaluated at $t_n - t_{\hat{n}}$.

For the pantograph interaction, we are interested in the displacement of the contact point $u_c(t_n) = u(t_n, \mathbf{x}_{cw}(t_n))$. Therefore, Eq. (20) can be evaluated at

15

this point as:

$$u_{\mathrm{c}}(t_n) = u(t_n, \mathbf{x}_{\mathrm{cw}}(t_n)) = \sum_{\hat{n}=0}^{N_{\mathrm{c}}-1} \mathbb{I}(n, \hat{n})\, f_{\mathrm{c}}(t_{\hat{n}}) \qquad (21)$$

in which:

$$\mathbb{I}(n, \hat{n}) = h(t_n - t_{\hat{n}}, \mathbf{x}_{\mathrm{cw}}(t_n), \mathbf{y}_{\mathrm{cw}}(t_{\hat{n}}))\Delta t \qquad (22)$$

In addition to the displacement due to interaction with the pantograph, the vertical position of the contact wire depends on the static configuration of the catenary. If $z_{\mathrm{cw}}(t_n)$ is the contact wire height at the initial catenary configuration, the global height of the contact point at time step n can be obtained, as shown in Fig. 4, from:

$$z_{\mathrm{c}}(t_n) = z_{\mathrm{cw}}(t_n) + u_{\mathrm{c}}(t_n) \qquad (23)$$

Eq. (21) condenses in a $N_{\mathrm{c}} \times N_{\mathrm{c}}$ matrix $\mathbb{I}(n, \hat{n})$ the steady-state vertical displacement of the contact point at time t_n as a function of the stationary force applied in all contact points of the block at time $t_{\hat{n}}$ for $\hat{n} = 0, ..., N_c - 1$. It is important to note that when the force is measured and applied at a given time step $\bar{n} \in \hat{n}$, the response for all the time steps n is affected.

Matrix $\mathbb{I}(n, \hat{n})$ can be precomputed making the proposed model very suitable for use in HIL testing because few operations are required to obtain the contact point response. We propose to apply this model in combination with an algorithm in which the measured contact force is iteratively updated until the steady-state response is achieved.

Defining k as the global counter of each step or iteration of the HIL test, at the beginning of the test ($k = 0$), a set of N_{c} (the number of contact points in a block) null values of the contact force are considered, so that $z_{\mathrm{c}}(t_n) = z_{\mathrm{cw}}(t_n)$. At a given iteration k, the contact force is measured at time step $\bar{n}$ relative to the beginning of the current block b. In this step, only the contact force values measured from t_0 to $t_{\bar{n}}$ are available in the current block. To complete the set of N_{c} measures of contact force required to compute the response of the catenary model, the contact force values from $t_{\bar{n}+1}$ to $t_{N_{\mathrm{c}}-1}$ are taken from the previous

16

block $b - 1$. Thus, by combining Eqs. (23) and (21) the contact point height in iteration k is computed as:

$$z_{\mathrm{c}}^k(t_n) = z_{\mathrm{cw}}(t_n) + \sum_{\hat{n}=0}^{\bar{n}} \mathbb{I}(n,\hat{n})\, f_{\mathrm{c}}^b(t_{\hat{n}}) + \sum_{\hat{n}=\bar{n}+1}^{N_{\mathrm{c}}-1} \mathbb{I}(n,\hat{n})\, f_{\mathrm{c}}^{b-1}(t_{\hat{n}}) \qquad (24)$$

Note that the response $z_{\mathrm{c}}(t_n)$, defined from t_0 to $t_{N_{\mathrm{c}}-1}$, must be updated for all t_n every iteration k.
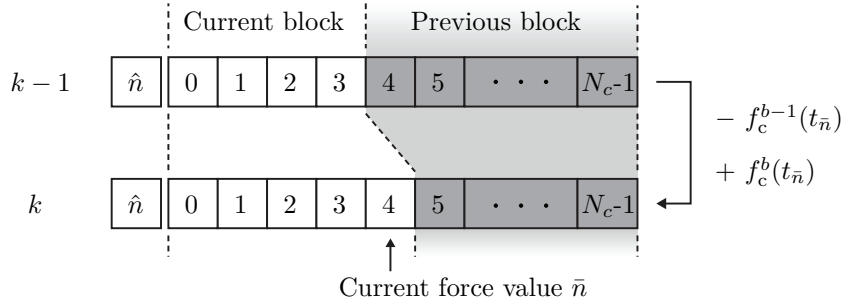
Figure 5: *Modification of the set of N_{c} force values by replacing $f_{\mathrm{c}}^{b-1}(t_{\bar{n}})$ by $f_{\mathrm{c}}^b(t_{\bar{n}})$ at two consecutive iterations.*

Eq. (24) can be rewritten based on the difference of the measured contact force of the current block and that of the same instant of the previous block. That is:

$$z_{\mathrm{c}}^k(t_n) = z_{\mathrm{c}}^{k-1}(t_n) + \mathbb{I}(n,\bar{n}) \left(f_{\mathrm{c}}^b(t_{\bar{n}}) - f_{\mathrm{c}}^{b-1}(t_{\bar{n}}) \right) \qquad (25)$$

This strategy is schematically illustrated at Fig. 5.

Once the contact wire height is available, only the vertical position of the contact point for the next time step $z_{\mathrm{c}}^k(t_{\bar{n}+1})$ is sent to the actuator. The method runs iteratively step by step until the measured contact force in two consecutive blocks matches with a given tolerance.

The methodology explained so far is exemplified in Appendix A by means of a very simple academic model that allows the numerical results to be better understood and reproduced.

5. Hardware in the loop method with nonlinear catenary model

The HIL procedure explained in Section 4 is now extended to include the non-linear behaviour of droppers. We use the same idea introduced in [25] but adapted to account for the periodic nature of the system. The proposed formulation is developed in two stages. In the first, the response is computed with assumption to the linear model described in Section 4. The second is devoted to apply correction forces to the slackened droppers.

5.1. Dropper correction forces

The static equilibrium problem in a catenary system is a non-linear problem governed by large displacements. However, the dynamic behaviour can be linearised around the static equilibrium position in which each dropper d has a tension value f_{d0} and a stiffness k_d in the dropper direction. Droppers are cables that cannot exert compression forces. However, these compression forces are considered in the linear catenary model in which the tension of dropper d is computed as $f = k_d \Delta L_d$ (dashed line in Fig. 6(a)). To satisfy the condition of no compression forces, the internal force of a dropper must be greater than $-f_{d0}$ (continuous line in Fig. 6(a)). Thus, a correction force f_d must be applied to correct the linear behaviour as shown in Fig. 6(a). This consists of two compression forces applied at both ends of the dropper $\mathbf{y}_{d,\mathrm{inf}}$ and $\mathbf{y}_{d,\mathrm{sup}}$, as depicted in Fig. 6(b).
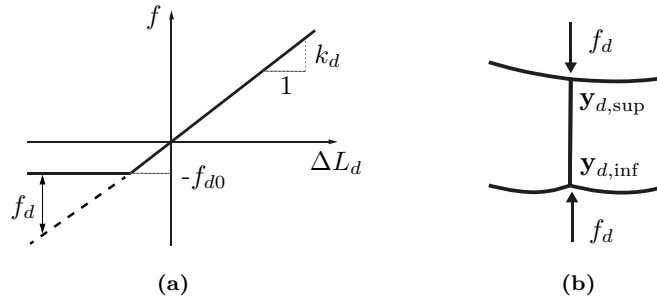
Figure 6: *(a) Non-linear behaviour of droppers. (b) Correction forces f_d applied on dropper d.*

18

In this subsection, we attempt to explain the influence which a periodic sequence of unitary impulses applied on contact points and dropper ends has on the displacement of these points.

We first define the dropper elongation ΔL_d as:

$$\Delta L_d = u(\mathbf{x}_{d,\text{sup}}) - u(\mathbf{x}_{d,\text{inf}}) \tag{26}$$

$\mathbb{I}(n, \hat{n})$ in Eq. (21) can be redefined as $\mathbb{I}_{\text{c}}^{\text{c}}(n, \hat{n})$ in which the subscript c denotes that the excitation is produced by the contact force and the superscript c indicates that the response is evaluated at the contact point. With this notation, the displacement of the contact point produced by the contact force defined in Eq. (21) is now renamed:

$$u_{\text{c}}^{\text{l}}(t_n) = \sum_{\hat{n}=0}^{N_{\text{c}}-1} \mathbb{I}_{\text{c}}^{\text{c}}(n, \hat{n}) \, f_{\text{c}}(t_{\hat{n}}) \tag{27}$$

Superscript l is used to point out the fact that this displacement is considered the linear part of the total response.

Dropper elongation due to the contact force is:

$$\Delta L_d^{\text{l}}(t_n) = \sum_{\hat{n}=0}^{N_{\text{c}}-1} \mathbb{I}_{\text{c}}^{d}(n, \hat{n}) \, f_{\text{c}}(t_{\hat{n}}) \tag{28}$$

in which:

$$\mathbb{I}_{\text{c}}^{d}(n, \hat{n}) = [h(t_n - t_{\hat{n}}, \mathbf{x}_{d,\text{sup}}, \mathbf{y}_{\text{cw}}(t_{\hat{n}})) - h(t_n - t_{\hat{n}}, \mathbf{x}_{d,\text{inf}}, \mathbf{y}_{\text{cw}}(t_{\hat{n}}))] \, \Delta t \tag{29}$$

To include the influence of dropper correction forces in the catenary response, we first assume that the dropper correction force $f_d(t_n)$ of dropper d at t_n is known. It is important to remark that the correction of the infinite droppers of the catenary model at all time steps should be considered because they affect the response on the contact point at time step $\bar{n}$. In practise however, dropper correction will not be considered in time instants at which the pantograph is far enough from the reference block because it is highly improbable that a dropper slackens and in such a case, its influence on the pantograph interaction has been

proven to be negligible. Thus, dropper correction is active only at time instants from $t_{-n_{\mathrm{b}}}$ to $t_{n_{\mathrm{a}}}$.

The displacement produced on the contact point due to dropper correction forces is called the non-linear part of the response (denoted by superscript nl) and is defined as:

$$u_{\mathrm{c}}^{\mathrm{nl}}(t_n) = \sum_{d=1}^{N_{\mathrm{d}}} \sum_{\hat{n}=-n_{\mathrm{b}}}^{n_{\mathrm{a}}} \mathbb{I}_d^{\mathrm{c}}(n, \hat{n}) \, f_d(t_{\hat{n}}) \tag{30}$$

in which N_{d} is the number of droppers of the reference block and

$$\mathbb{I}_d^{\mathrm{c}}(n, \hat{n}) = \left[h(t_n - t_{\hat{n}}, \mathbf{x}_{\mathrm{cw}}(t_n), \mathbf{y}_{d,\mathrm{inf}}) - h(t_n - t_{\hat{n}}, \mathbf{x}_{\mathrm{cw}}(t_n), \mathbf{y}_{d,\mathrm{sup}}) \right] \Delta t \tag{31}$$

Dropper d elongation caused by the correction forces applied to dropper $\hat{d}$ are computed from:

$$\Delta L_d^{\mathrm{nl}}(t_n) = \sum_{\hat{d}=1}^{N_{\mathrm{d}}} \sum_{\hat{n}=-n_{\mathrm{b}}}^{n_{\mathrm{a}}} \mathbb{I}_{\hat{d}}^{d}(n, \hat{n}) \, f_{\hat{d}}(t_{\hat{n}}) \tag{32}$$

being

$$\begin{aligned} \mathbb{I}_{\hat{d}}^{d}(n, \hat{n}) = {} & \left[h(t_n - t_{\hat{n}}, \mathbf{x}_{d,\mathrm{sup}}, \mathbf{y}_{\hat{d},\mathrm{inf}}) - h(t_n - t_{\hat{n}}, \mathbf{x}_{d,\mathrm{sup}}, \mathbf{y}_{\hat{d},\mathrm{sup}}) \right] \Delta t \\ & - \left[h(t_n - t_{\hat{n}}, \mathbf{x}_{d,\mathrm{inf}}, \mathbf{y}_{\hat{d},\mathrm{inf}}) - h(t_n - t_{\hat{n}}, \mathbf{x}_{d,\mathrm{inf}}, \mathbf{y}_{\hat{d},\mathrm{sup}}) \right] \Delta t \end{aligned} \tag{33}$$

The total response can be obtained by adding the linear (l) and non-linear (nl) contributions defined above.

5.3. HIL with dropper correction forces

The same procedure as that defined in Section 4 is used here but now, dropper correction forces are added to the system. It is important to highlight that dropper correction forces can be applied at instants before and after the time instants at which the pantograph stays within the domain of the block ($t_{\hat{n}}$ for $\hat{n} = 0, ..., N_{\mathrm{c}} - 1$).

At a given iteration k, the first step consists of updating the response due to the contact force measured at $t_{\bar{n}}$ as in Eq. (25):

$$u_{\mathrm{c}}^{\mathrm{l},k}(t_n) = u_{\mathrm{c}}^{k-1}(t_n) + \mathbb{I}_{\mathrm{c}}^{\mathrm{c}}(n, \bar{n}) \left(f_{\mathrm{c}}^{b}(t_{\bar{n}}) - f_{\mathrm{c}}^{b-1}(t_{\bar{n}}) \right) \tag{34}$$

20

In this case, it is also necessary to update the elongation of droppers due to this contact force:

$$\Delta L_d^{1,k}(t_n) = \Delta L_d^{k-1}(t_n) + \mathbb{I}_c^d(n, \bar{n}) \left(f_c^b(t_{\bar{n}}) - f_c^{b-1}(t_{\bar{n}}) \right) \tag{35}$$

The second stage consists of modifying the response according to the effect of dropper correction forces. Note that the dropper corrections forces $f_d(t_{\hat{n}})$ are applied at time instants $t_{\hat{n}}$ for $\hat{n} = -n_b, ..., n_a$ (a bigger interval than $[0, N_c-1]$). Thus, at every iteration k, f_d must be calculated in several instants in order to include all the instants from $-n_b$ to n_a. For example, if $-n_b = -N_c$ and $n_a = 2N_c-1$, which means that dropper correction is active since the pantograph gets into the previous block $(b = -1)$ until the pantograph gets off the next block $(b = 1)$, f_d must be computed and applied at three instants of time, namely $t_{\bar{n}}$, $t_{\bar{n}-N_c}$ and $t_{\bar{n}+N_c}$.

The effect of dropper correction forces modifies the linear response defined in Eqs. (34) and (35) so that:

$$u_c^k(t_n) = u_c^{1,k}(t_n) + \sum_{d=1}^{N_d} \sum_{\hat{n}=\bar{n}_d} \mathbb{I}_d^c(n, \hat{n}) \left(f_d^b(t_{\hat{n}}) - f_d^{b-1}(t_{\hat{n}}) \right) \tag{36}$$

$$\Delta L_d^k(t_n) = \Delta L_d^{1,k}(t_n) + \sum_{\hat{d}=1}^{N_d} \sum_{\hat{n}=\bar{n}_d} \mathbb{I}_{\hat{d}}^d(n, \hat{n}) \left(f_{\hat{d}}^b(t_{\hat{n}}) - f_{\hat{d}}^{b-1}(t_{\hat{n}}) \right) \tag{37}$$

in which $\bar{n}_d$ considers all the instants included into $[-n_b, n_a]$ that are spaced N_c steps from the current measuring time $\bar{n}$. For the choice of $-n_b$ and n_a indicated above, $\bar{n}_d = [\bar{n}, \bar{n} - N_c, \bar{n} + N_c]$. This is equivalent to applying this correction to the droppers of the previous and next blocks at the current instant $t_{\bar{n}}$.

At this point, the dropper correction forces $f_d^b(t_{\bar{n}_d})$ are the only magnitudes left to calculate to know the response at iteration k. First, we must find out the droppers to which the correction must be applied. To this end, the dropper state $\mathbb{O}_d^k$ defines the slackening state of dropper d, being equal to 0 if the dropper

21

is tensed and 1 if it is slackened. At time $\bar{n}_{\mathrm{d}}$, it reads:

$$\mathbb{O}_d^k(t_{\bar{n}_{\mathrm{d}}}) = \begin{cases} 0 & \text{if} \quad k_d \ \Delta L_d^{1,k}(t_{\bar{n}_{\mathrm{d}}}) \geq -f_{d0} \\ 1 & \text{if} \quad k_d \ \Delta L_d^{1,k}(t_{\bar{n}_{\mathrm{d}}}) < -f_{d0} \end{cases} \tag{38}$$

in which $\Delta L_d^{1,k}(t_{\bar{n}_{\mathrm{d}}})$ is obtained from Eq. (35).

As shown in Fig. 6(a), the dropper correction force can be written as:

$$f_d^b(t_{\bar{n}_{\mathrm{d}}}) = \mathbb{O}_d^k(t_{\bar{n}_{\mathrm{d}}}) \left(-f_{d0} - k_d \Delta L_d^k(t_{\bar{n}_{\mathrm{d}}}) \right) \tag{39}$$

According to Eq. (37), the previous equation becomes:

$$f_d^b(t_{\bar{n}_{\mathrm{d}}}) = \mathbb{O}_d^k(t_{\bar{n}_{\mathrm{d}}}) \Bigg(-f_{d0} - k_d \Bigg(\Delta L_d^{1,k}(t_{\bar{n}_{\mathrm{d}}}) + \\ \sum_{\hat{d}=1}^{N_{\mathrm{d}}} \sum_{\hat{n}=\bar{n}_{\mathrm{d}}} \mathbb{I}_{\hat{d}}^d(\bar{n}_{\mathrm{d}}, \hat{n}) \left(f_{\hat{d}}^b(t_{\hat{n}}) - f_{\hat{d}}^{b-1}(t_{\hat{n}}) \right) \Bigg) \Bigg) \tag{40}$$

This is a system of $N_{\mathrm{d}} \times N_{\bar{n}_{\mathrm{d}}}$ linear equations that allows to calculate the dropper correction forces $f_d^b(t_{\bar{n}_{\mathrm{d}}})$. Note that $N_{\bar{n}_{\mathrm{d}}}$ is the number of time steps included in $\bar{n}_{\mathrm{d}}$ and the system is in practice reduced since some of the equations become $f_d^b(t_{\bar{n}_{\mathrm{d}}}) = 0$ because dropper correction is not active in dropper d at some instants considered in $\bar{n}_{\mathrm{d}}$.

The final response at iteration k, including dropper correction, is calculated with Eqs. (36) and (37). Dropper state can change once the correction is applied but it is not necessary to recalculate it. If the convergence is achieved after several blocks, the difference between the response in two consecutive blocks tends to zero and the stationary dropper state is achieved.

6. Numerical results

In this section, the algorithm proposed is tested in a virtual HIL simulation in which a numerical pantograph model is used to replace the real pantograph used in a standard HIL test. The time integration of the pantograph model is carried out independently of the catenary model by means of the Hilber-Hughes-Taylor (HHT) integration method [27]. In this virtual test, the displacement of

22

the catenary contact point obtained from Eq. (36) is imposed on the pantograph model and the contact force in the next time step is computed. Unlike in a real HIL test in which this force would be measured by load cells, in the simulated test, a penalty stiffness is used [2].

To validate the method, the results obtained in the virtual HIL test are compared with a FEM conventional simulation. It is noteworthy to mention that the virtual HIL test assumes an infinite periodic catenary while the size of conventional FEM model is limited by the number of degrees of freedom. However, we have made a long enough catenary section so that the steady-state regime can be assumed on its central spans. In this way, transient effects are negligible due to the notable length of the FEM catenary model and it is expected to obtain the same solution in both the proposed periodic model (PFEM), and the finite length FEM model.

Specifically, in this example, we chose the catenary model used in the benchmark exercise [2] with spans (or blocks) of 55 m in length having 9 droppers and 55 mm of pre-sag in the contact wire each of them. A Rayleigh damping model is used with $\mathbf{C} = \beta \mathbf{K} + \gamma \mathbf{M}$, being $\beta = 10^{-4}$ s and $\gamma = 1.25 \cdot 10^{-2}$ s^{-1}. For the pantograph, a lumped mass model with 3 vertical degrees of freedom is used whose parameters are provided in Table 1. The penalty stiffness used in the contact model is $k_h = 50000$ N/m according to [2].

Table 1: *Parameters of the pantograph model.*

d.o.f.	m(kg)	c(Ns/m)	k(N/m)
1	6.6	0	7000
2	5.8	0	14100
3	5.8	70	80

In the PFEM, the catenary impulse responses have to be computed for a discrete number of frequencies (see Eq. (17)). We have found that $\Delta\omega = 0.025$ rad/s with a maximum frequency $\omega_{max} = 750$ rad/s are accurate enough values.

23

Note that the frequency resolution $\Delta\omega$ must be small enough to guarantee a large period $2\pi/\Delta\omega$ of the functions to which the DFT is applied. In turn, the maximum frequency involved in the IDFT must be high enough to provide a fine time discretisation of the nodal forces. The time resolution is chosen to $\Delta t = 1$ ms, a value which is smaller than π/ω_{max} to avoid aliasing effects. This value is also used for time integration of the pantograph model, although in this case, a smaller value could be used.

In the numerical case analysed in this section, the velocity of the pantograph is set at 250 km/h and the virtual HIL simulation runs until there is not noticeable differences in the computed contact force of two consecutive blocks. To ease convergence of the virtual HIL test, during the first 20 s of the simulation, the displacement of the catenary contact point that is imposed on the pantograph model is scaled by a factor that increases linearly from 0 to 1. This is reflected in the increasing values in the first blocks of the results shown in this example (see Fig. 7 and Fig. 8).
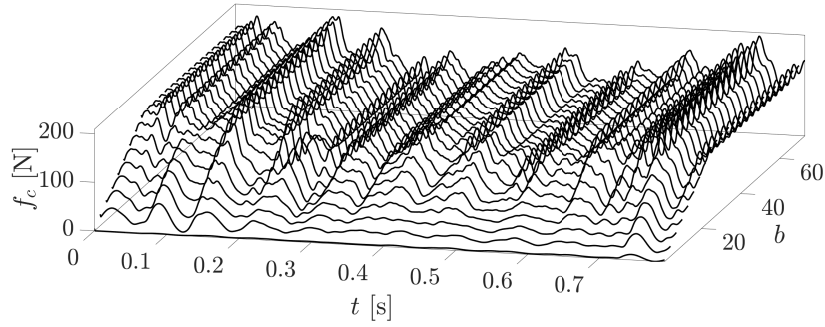

Figure 7: *Contact force evolution.*

24
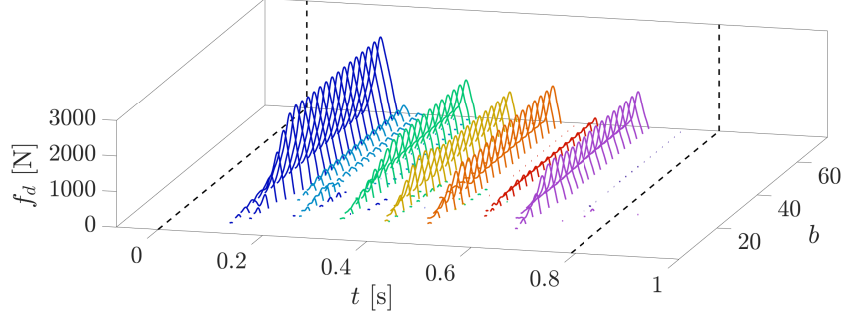
Figure 8: *Dropper correction forces evolution.*

The contact force obtained in successive blocks of the virtual test is depicted in Fig. 7 in which only one in three curves are shown for a better visualisation of the figure. The non-linear correction forces of droppers 2 to 8 (Eq. (39)) can be seen in Fig. 8 from left to right and again one in three curves are displayed. Note that the first and last droppers do not present any correction force since they do not slacken due to their greater initial tensile force caused by the pre-sag of the contact wire. The two black dashed lines show the times in which the pantograph is placed inside the reference block from $t = 0$ to $t = 0.792$ s. However, dropper correction forces are also computed outside this period but they are null in this example. Specifically, the period in which dropper correction is active covers two blocks, from step $-n_b = 80$ to $n_a = 1504$.

As seen in both figures, convergence is properly achieved, although it is important to mention that some convergence issues can arise if the periodic structure is very low damped. Thus, a certain amount of damping is required to guarantee the convergence of the proposed approach.

In order to validate the results, the converged contact force obtained from the catenary PFEM is compared in Fig. 9 with the contact force of three consecutive central blocks computed with a conventional FEM simulation. We have used two catenary models with different length, namely 15 and 30 spans respectively. The FEM solutions show minor differences with the contact force obtained from

25
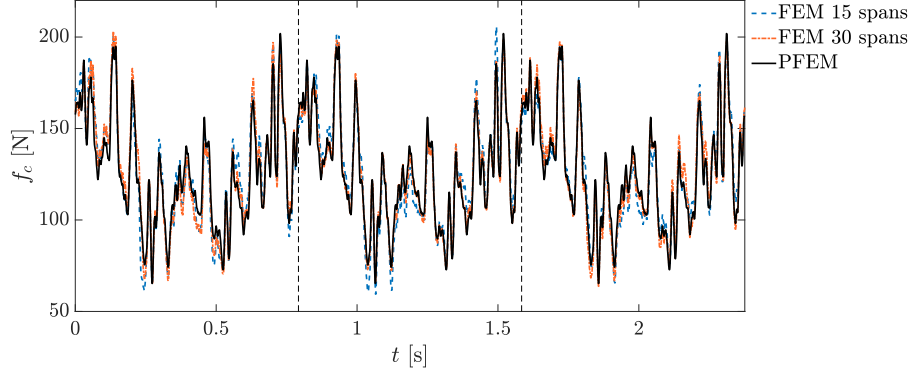
Figure 9: *Comparison of contact force of catenary PFEM (solid line) with those obtained in three central spans of the section of a FE catenary model with 15 spans (dashed line) and 30 spans (dash-dotted line).*

the PFEM. These differences are even smaller with the 30-spans FE catenary model because a more stationary response is achieved on these central spans. The converged dropper correction forces obtained from the catenary PFEM are also compared with those obtained from the longest FE catenary model in Fig. 10. As can be seen in both figures, the results provided by the proposed catenary PFEM are validated according to their great similarities with those obtained from a FEM simulation with a large enough catenary model.

26
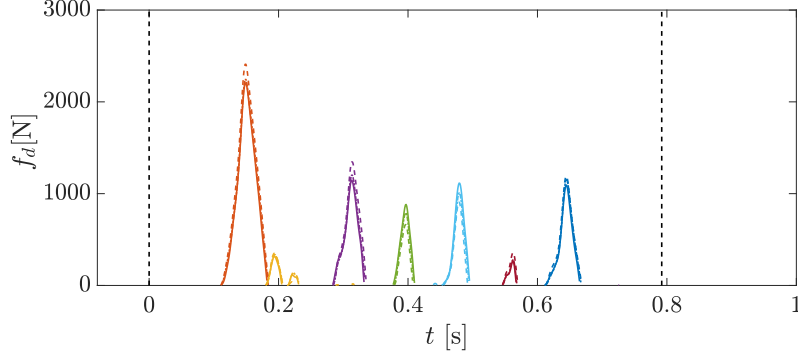
Figure 10: *Comparison of dropper correction forces from catenary PFEM (solid lines) with those obtained in a central span of a FE catenary model with 30 spans (dashed lines).*

Regarding the computational cost required to obtain the PFEM solution, a distinction must be made between the *off-line* and *on-line* stages. The former takes a relatively long computation time which mainly includes the FRF of the catenary periodic block and the unitary impulse response functions. Specifically, for the example previously analysed, it takes approximately 30 minutes in a conventional computer.

The *on-line* stage covers the computations that must fulfil real-time performance to perform HIL tests. For a given time-step t_n, the measured contact force is taken as input and the contact point height must be given before the next contact force is measured. The operations involved are described in Table 2.

For the numerical example previously analysed in which $\Delta t = 1$ ms, $N_c = 792$, $N_{\bar{n}_d} = 2$, $N_d = 9$ and N_{sd} ranges from 0 to N_d. With these values, that can be taken as usual, the operations involved in each time step need about 0.15 ms to be performed, which confirms the real-time capability of the proposed formulation and its potential use for HIL pantograph tests.

27

Table 2: *Operations performed in a given time step in the on-line stage.*

Equation	Description	Operations
Eq. (34)	Contact point displacement due to contact force.	$[\ ]_{N_c \times 1} + \Delta f_c \cdot [\ ]_{N_c \times 1}$
Eq. (35)	Droppers elongation due to contact force.	$[\ ]_{N_c \cdot N_{\bar{n}_d} \cdot N_d \times 1} + \Delta f_c \cdot [\ ]_{N_c \cdot N_{\bar{n}_d} \cdot N_d \times 1}$
Eq. (38)	Dropper state.	$k_d \cdot [\ ]_{N_c \cdot N_{\bar{n}_d} \cdot N_d \times 1} < -f_{d0} \quad d = 1, ..., N_d$
Eq. (40)	Slackened droppers correction force.	$[\ ]_{N_{sd} \times N_{sd}}^{-1} \cdot [\ ]_{N_{sd} \times 1}$
Eq. (36)	Contact point displacement due to slackened droppers correction force.	$[\ ]_{N_c \times 1} + [\ ]_{N_c \times N_{sd}} \cdot \Delta f_d$
Eq. (37)	Droppers elongation due to slackened droppers correction force.	$[\ ]_{N_c \cdot N_{\bar{n}_d} \cdot N_d \times 1} + [\ ]_{N_c \cdot N_{\bar{n}_d} \cdot N_d \times N_{sd}} \cdot \Delta f_d$

7. Conclusions

In this paper, we present a whole framework to perform HIL pantograph tests achieving the steady state of the pantograph-catenary dynamic interac-tion. The contribution of this paper is twofold: on the one hand we proposed the formulation to build an infinite periodic structure model, discretised by the FEM and subjected to a moving load travelling at constant velocity. The PFEM formulation is directly built from the common FE matrices that define the repet-itive block of the system, so that it is valid for any generic periodic structure. The proposed formulation has been applied to compute the impulse response

28

of a railway catenary PFEM to be subsequently used in HIL pantograph tests. On the other hand, an iterative strategy to achieve the steady state when the the catenary PFEM is used in HIL pantograph tests is proposed and numerically validated, even with the extension of the method in which the non-linear behaviour of droppers is also considered.

The main conclusions that can be drawn from this work are:

- From the FE model of a given infinite periodic structure repetitive block and applying periodic boundary conditions, it has been verified, by means of standard simulations with a very long FE catenary model, that the proposed catenary PFEM provides the precise steady-state response under a constant velocity moving load.

- The catenary PFEM requires very low computational cost which allows its implementation in HIL tests, in which real-time performance is mandatory. Even when the non-linear behaviour of droppers is included into the algorithm, it is still able to be solved in real time.

- Although it is unavoidable to manage a delay produced in the communication and execution of the control loop of the actuator, the proposed formulation has the advantage of being able of easily compensate this delay since the response for a later time is available at the current time step.

- The proposed framework to perform HIL tests with the catenary PFEM only focuses on the steady-state response and therefore, other particularities of the pantograph-catenary interaction such as contact wire irregularities, uneven spans or overlaps can not be addressed.

Future work will lead to the implementation of the proposed method in a HIL test rig, in which the stability of the method needs to be checked in the presence of experimental issues such as noise, delays, limited measuring accuracy, vibrations and so on. Additionally, the catenary PFEM can be extended

29

to consider the interaction with two pantographs offering the opportunity of studying the interference phenomenon between pantographs.

Acknowledgements

References

[1] S. Bruni, G. Bucca, M. Carnevale, A. Collina, A. Facchinetti, Pantograph–catenary interaction: recent achievements and future research challenges, International Journal of Rail Transportation 6 (2) (2018) 57–82. `doi:10.1080/23248378.2017.1400156`.

[2] S. Bruni, J. Ambrosio, A. Carnicero, Y. H. Cho, L. Finner, M. Ikeda, S. Y. Kwon, J. P. Massat, S. Stichel, M. Tur, The results of the pantograph-catenary interaction benchmark, *Veh Syst. Dyn.* 53 (3) (2015) 412–435. `doi:10.1080/00423114.2014.953183`.

[3] W. Song, C.-M. Chang, V. K. Dertimanis, Editorial: Recent advances and applications of hybrid simulation, Frontiers in Built Environment 6 (2020). `doi:10.3389/fbuil.2020.625197`.

[4] A. Facchinetti, S. Bruni, Hardware-in-the-loop hybrid simulation of pantograph–catenary interaction, Journal of Sound and Vibration 331 (12) (2012) 2783–2797. `doi:10.1016/j.jsv.2012.01.033`.

[5] Y. Song, Z Liu, A. Ronnquist, P Navik, Z Liu, Contact wire irregularity stochastics and effect on high-speed railway pantograph–catenary interac-tions, IEEE Transactions on Instrumentation and Measurement 69 (10) (2020) 8196–8206. `doi:10.1109/TIM.2020.2987457`.

[6] S. Gregori, J. Gil, M. Tur, J. Tarancón, F. Fuenmayor, Analysis of the overlap section in a high-speed railway catenary by means of numerical simulations, Engineering Structures 221 (2020) 110963. `doi:10.1016/j.engstruct.2020.110963`.

[7] H. Ouyang, Moving-load dynamic problems: A tutorial (with a brief overview), Mechanical Systems and Signal Processing 25 (6) (2011) 2039–2060, interdisciplinary Aspects of Vehicle Dynamics. `doi:https://doi.org/10.1016/j.ymssp.2010.12.010`.

[8] D. J. Mead, Vibration response and wave propagation in periodic structures, *J. Eng. Ind.* 93 (3) (1971) 783–792. `doi:10.1115/1.3428014`.

[9] C. Cai, Y. Cheung, H. Chan, Dynamic response of infinite continuous beams subjected to a moving force – An exact method, *J. Sound Vib.* 123 (3) (1988) 461 – 472. `doi:10.1016/S0022-460X(88)80163-9`.

[10] P. Belotserkovskiy, On the oscillations of infinite periodic beams subjected to a moving concentrated force, *J. Sound Vib.* 193 (3) (1996) 705 – 712. `doi:10.1006/jsvi.1996.0309`.

[11] A. Metrikine, A. Bosch, Dynamic response of a two-level catenary to a moving load, *J. Sound Vib.* 292 (3) (2006) 676 – 693. `doi:10.1016/j.jsv.2005.08.026`.

[12] X. Sheng, C. Jones, D. Thompson, Responses of infinite periodic structures to moving or stationary harmonic loads, *J. Sound Vib.* 282 (2005) 125–149. `doi:10.1016/j.jsv.2004.02.050`.

[13] X. Sheng, C. Jones, D. Thompson, Using the fourier-series approach to study interactions between moving wheels and a periodically supported rail, *J. Sound Vib.* 303 (2007) 873–894. `doi:10.1016/j.jsv.2007.02.007`.

[14] J.-M. Mencik, On the low- and mid-frequency forced response of elastic structures using wave finite elements with one-dimensional propagation, *Comput. Struct.* 88 (11) (2010) 674 – 689. `doi:10.1016/j.compstruc.2010.02.006`.

[15] B. Claudet, T. Hoang, D. Duhamel, G. Foret, J.-L. Pochet, F. Sabatier, Wave finite element method for computing the dynamic response of railway transition zones subjected to moving loads, in: *COMPDYN 2019*, Crete, Greece, 2019, pp. 4538–4547. `doi:10.7712/120119.7247.18688`.

[16] T. Hoang, D. Duhamel, G. Forêt, J.-L. L. Pochet, F. Sabatier, Wave finite element method and moving loads for the dynamic analysis of railway tracks, in: *WCCM XIII*, New York, United States, 2018.

[17] W. Zhang, G. Mei, X. Wu, Z. Shen, Hybrid simulation of dynamics for the pantograph-catenary system, *Veh. Syst. Dyn.* 38 (6) (2002) 393–414. `doi:10.1076/vesd.38.6.393.8347`.

[18] W. Zhang, G. Mei, X. Wu, L. Chen, A study on dynamic behaviour of pantographs by using hybrid simulation method, *Proc. Inst. Mech. Eng. F: J. Rail Rapid Transit* 219 (3) (2005) 189–199. `doi:10.1243/095440905X8880`.

[19] A. Collina, A. Facchinetti, F. Fossati, F. Resta, Hardware in the loop test-rig for identification and control application on high speed pantographs, *Shock Vib.* 11 (2004) 445–456. `doi:10.1155/2004/740146`.

[20] F. Resta, A. Facchinetti, A. Collina, G. Bucca, On the use of a hardware in the loop set-up for pantograph dynamics evaluation, *Veh. Syst. Dyn,* 46 (S1) (2008) 1039–1052. `doi:10.1080/00423110802037891`.

[21] A. Facchinetti, M. Mauri, Hardware-in-the-loop overhead line emulator for active pantograph testing, *IEEE Trans. Ind. Electron.* 56 (10) (2009) 4071–4078. `doi:10.1109/TIE.2009.2023632`.

[22] A. Schirrer, G. Aschauer, E. Talic, M. Kozek, S. Jakubek, Catenary emulation for hardware-in-the-loop pantograph testing with a model predictive energy-conserving control algorithm, *Mechatronics* 41 (2017) 17 – 28. `doi:10.1016/j.mechatronics.2016.11.002`.

[23] S. Gregori, M. Tur, A. Pedrosa, J. Tarancón, F. Fuenmayor, A modal coordinate catenary model for the real-time simulation of the pantograph-catenary dynamic interaction, Finite Elements in Analysis and Design 162 (2019) 1–12.

[24] J. Gil, M. Tur, A. Correcher, S. Gregori, A. Pedrosa, F. J. Fuenmayor, Hardware-in-the-loop pantograph tests using analytical catenary models, *Veh Syst. Dyn.* (2021) 1–15`doi:10.1080/00423114.2021.1962538`.

[25] S. Gregori, M. Tur, E. Nadal, J. V. Aguado, F. J. Fuenmayor, F. Chinesta, Fast simulation of the pantograph–catenary dynamic interaction, *Finite Elem. Anal. Des.* 129 (2017) 1 – 13. `doi:10.1016/j.finel.2017.01.007`.

[26] H. Chebli, R. Othman, D. Clouteau, Response of periodic structures due to moving loads, *Comptes Rendus Mécanique* 334 (6) (2006) 347 – 352. `doi:10.1016/j.crme.2006.04.001`.

[27] H. M. Hilber, T. J. Hughes, R. L. Taylor, Improved numerical dissipation for time integration algorithms in structural dynamics, *Earthq. Eng. Struct. Dyn.* 5 (3) (1977) 283–292. `doi:10.1002/eqe.4290050306`.

Appendix A. Demonstrative example

In order to illustrate the method and facilitate the reproducibility of the numerical results, a HIL simulation is described in this appendix by using a linear small-size FE model. The procedure described in the paper is thoroughly followed and some numerical results are provided at each step.
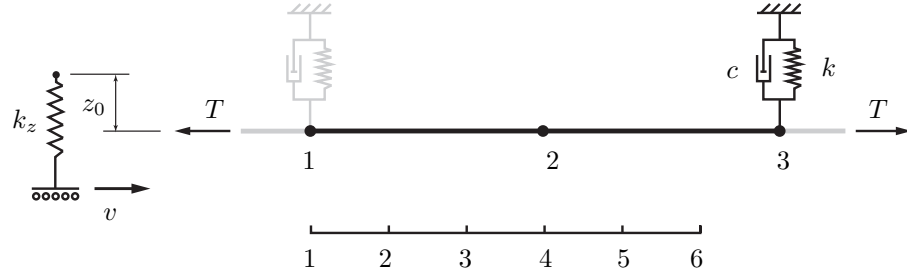
Figure A.11: *Academic periodic FE model.*

The infinite periodic model chosen is composed of a tensioned string periodically supported as shown in Fig. A.11. The repeated block consists of a piece of string modelled with two elements (3 nodes) and a spring-damper system on the right end. A given element of the string has two nodes and two degrees of freedom, the vertical displacement of each node. The dynamic equation of an

34

element e with tension T, linear density μ and length L_e is:

$$\mathbf{m}\ddot{\mathbf{u}}^{\text{e}} + \mathbf{k}\mathbf{u}^{\text{e}} = \mathbf{F}^{\text{e}} \tag{A.1}$$

in which the mass and stiffness matrices and the vector of degrees of freedom are:

$$\mathbf{m} = \frac{\mu L_e}{6}\begin{bmatrix} 2 & 1 \\ 1 & 2 \end{bmatrix}; \quad \mathbf{k} = \frac{T}{L_e}\begin{bmatrix} 1 & -1 \\ -1 & 1 \end{bmatrix}; \quad \mathbf{u}^{\text{e}} = \begin{bmatrix} u_1 \\ u_2 \end{bmatrix} \tag{A.2}$$

The FE model of the whole block is obtained by assembling the two string elements and the spring-damper system, which results in:

$$\mathbf{M} = \begin{bmatrix} \dfrac{\mu L_e}{3} & \dfrac{\mu L_e}{6} & 0 \\ \dfrac{\mu L_e}{6} & 2\dfrac{\mu L_e}{3} & \dfrac{\mu L_e}{6} \\ 0 & \dfrac{\mu L_e}{6} & \dfrac{\mu L_e}{3} \end{bmatrix}; \quad \mathbf{C} = \begin{bmatrix} 0 & 0 & 0 \\ 0 & 0 & 0 \\ 0 & 0 & c \end{bmatrix}; \tag{A.3}$$

$$\mathbf{K} = \begin{bmatrix} \dfrac{T}{L_e} & -\dfrac{T}{L_e} & 0 \\ -\dfrac{T}{L_e} & 2\dfrac{T}{L_e} & -\dfrac{T}{L_e} \\ 0 & -\dfrac{T}{L_e} & \dfrac{T}{L_e}+k \end{bmatrix}; \quad \mathbf{U} = \begin{bmatrix} u_1 \\ u_2 \\ u_3 \end{bmatrix}; \tag{A.4}$$

The numerical values of the parameters that define the model are shown in Table A.3. The time and frequency discretization is made with $\Delta t = 5$ ms and $\Delta\omega = 2\pi/(N\Delta t)$ rad/s, being $N = 10000$ and the number of harmonics $N_f = 5969$, which leads to a maximum frequency of ≈ 750 rad/s.

Table A.3: *Parameters of the academic model.*

| T(N)	μ(kg/m)	L_e(m)	k(N/m)	c(Ns/m)	v(m/s)
22000	1.3	0.75	300	10	50

The dynamic stiffness matrix $\mathbf{D}(\omega_k)$ can be computed with Eq. (6) and, by using Eqs. (12) and (14), the Frequency Response Function $\mathbf{H}(\omega_k)$ is obtained considering that node 1 is the left node, node 2 is the inner node and node 3 is the right node. For each frequency ω_k, $\mathbf{H}(\omega_k)$ is a matrix with two columns

related to the excitation on the inner and the right nodes and three rows that match to the displacement of each of the three nodes. For example, the matrix $\mathbf{H}(\omega_k)$ for the frequency index $k = 3000$ (60 Hz) is:

$$\mathbf{H}(\omega_{k=3000}) = 10^{-4} \begin{bmatrix} -0.1113 + 0.0845\ \mathrm{i} & 0.0161 - 0.0532\ \mathrm{i} \\ 0.0549 - 0.0074\ \mathrm{i} & -0.1113 + 0.0845\ \mathrm{i} \\ -0.1147 - 0.0797\ \mathrm{i} & 0.0555 - 0.0012\ \mathrm{i} \end{bmatrix}$$

Additionally, the norm of the different elements in $\mathbf{H}(\omega_k)$ are depicted in Fig. A.12, in which $|\mathbf{H}_{12}(\omega_k)| = |\mathbf{H}_{32}(\omega_k)|$ and $|\mathbf{H}_{11}(\omega_k)| = |\mathbf{H}_{22}(\omega_k)| = |\mathbf{H}_{31}(\omega_k)|$ due to the properties of the receptance and the periodic boundary conditions.
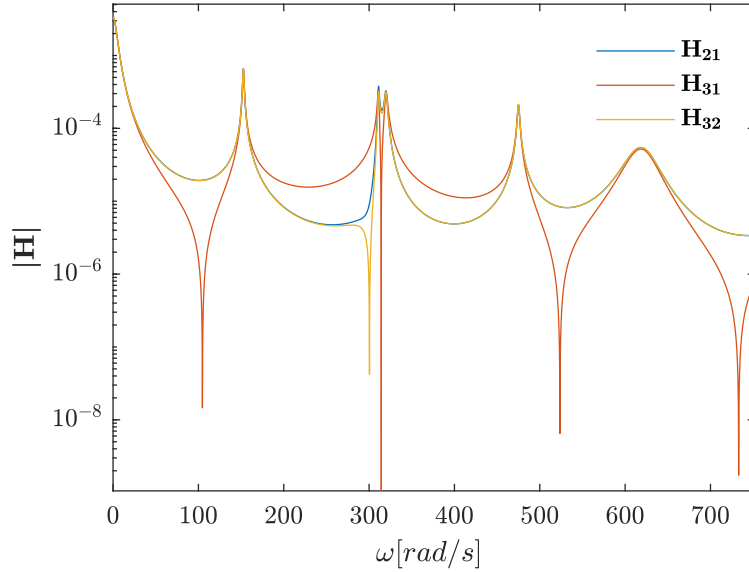
Figure A.12: *Norm of the receptance $H(\omega)$.*

The velocity of the moving load used in this example is $v = 50$ m/s. According to this value, the length of the block and Δt, there are $N_c = 6$ different discrete contact points along the block as depicted in Fig. A.11. The dynamic behaviour of the PFEM with a moving load is collected in the operator $\mathbb{I}(n, \hat{n})$. This operator is obtained with the evaluation of the discrete impulse function defined in Eq. (19) for all the combinations of $n \in [1, N_c]$ and $\hat{n} \in [1, N_c]$ as

36

stated in Eq. (22). As the continuous operator $I(\omega, \mathbf{x}, \mathbf{y})$ appears in the discrete impulse function (Eq. (19)), it also must be evaluated for all combinations of n and $\hat{n}$ considering that the observation point $\mathbf{x}$ is related to n and the excitation point $\mathbf{y}$ is related to $\hat{n}$. Thus, $I(\omega, n, \hat{n}) = I(\omega, \mathbf{x}_n, \mathbf{y}_{\hat{n}})$ is computed for every frequency ω_k, with 6 points of excitation and 6 points of observation, by means of Eq. (16).

To compute $I(\omega, n, \hat{n})$, the shape functions are arranged in a matrix that relates the forces of discrete points $\hat{n}$ (rows) to the three degrees of freedom (columns):

$$\mathbf{N} = \begin{bmatrix} 1 & 0 & 0 \\ 0.6667 & 0.3333 & 0 \\ 0.3333 & 0.6667 & 0 \\ 0 & 1 & 0 \\ 0 & 0.6667 & 0.3333 \\ 0 & 0.3333 & 0.6667 \end{bmatrix} \tag{A.5}$$

The operator $I(\omega, n, \hat{n})$ is organised in a matrix $\mathbf{I}$, referring the rows to n and the columns to $\hat{n}$. For example, the values of this operator for the frequency defined by $k = 3000$ are:

$$\mathrm{Re}(\mathbf{I}(\omega_{k=3000})) =$$

$$10^{-4} \cdot \begin{bmatrix} 0.0555 & -0.0001 & -0.0557 & -0.1113 & -0.0688 & -0.0264 \\ -0.0012 & -0.0195 & -0.0377 & -0.0559 & -0.0461 & -0.0362 \\ -0.0580 & -0.0388 & -0.0197 & -0.0005 & -0.0233 & -0.0461 \\ -0.1147 & -0.0582 & -0.0016 & 0.0549 & -0.0005 & -0.0559 \\ -0.0704 & -0.0475 & -0.0246 & -0.0016 & -0.0197 & -0.0377 \\ -0.0261 & -0.0368 & -0.0475 & -0.0582 & -0.0388 & -0.0195 \end{bmatrix}$$

$\text{Im}(\mathbf{I}(\omega_{k=3000})) =$

$$10^{-5} \cdot \begin{bmatrix} 0.0116 & -0.2738 & -0.5593 & -0.8448 & -0.3860 & 0.0728 \\ 0.2736 & 0.0028 & -0.2679 & -0.5387 & -0.3348 & -0.1310 \\ 0.5355 & 0.2795 & 0.0235 & -0.2325 & -0.2837 & -0.3348 \\ 0.7975 & 0.5562 & 0.3149 & 0.0736 & -0.2325 & -0.5387 \\ 0.3568 & 0.3429 & 0.3289 & 0.3149 & 0.0235 & -0.2679 \\ -0.0838 & 0.1295 & 0.3429 & 0.5562 & 0.2795 & 0.0028 \end{bmatrix}$$

To show more information of this operator, the elements of the first column are plotted in Fig. A.13 for every frequency. In this case, $|\mathbb{I}_{51}| = |\mathbb{I}_{31}|$ and $|\mathbb{I}_{61}| = |\mathbb{I}_{21}|$ due to the periodicity condition and the symmetry of the model.
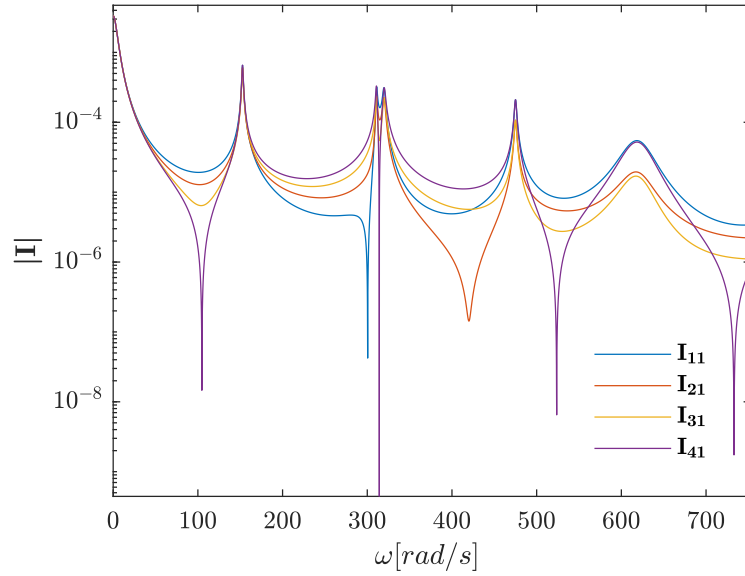
Figure A.13: *Harmonic response of discrete points of the block when the excitation is applied on point number 1.*

Finally, with Eq. (19) and Eq. (22), $\mathbb{I}(n, \hat{n})$ can be computed from $I(\omega, n, \hat{n})$.

In this case, it results in:

$$\mathbb{I} = 10^{-4} \begin{bmatrix} 0.3804 & 0.3934 & 0.4126 & 0.3758 & 0.4676 & 0.4853 \\ 0.4853 & 0.3735 & 0.3778 & 0.4197 & 0.4216 & 0.4319 \\ 0.4676 & 0.4439 & 0.3676 & 0.3934 & 0.4029 & 0.4216 \\ 0.3758 & 0.4750 & 0.4902 & 0.3627 & 0.3934 & 0.4197 \\ 0.4126 & 0.4200 & 0.4437 & 0.4902 & 0.3676 & 0.3778 \\ 0.3934 & 0.3913 & 0.4200 & 0.4750 & 0.4439 & 0.3735 \end{bmatrix}$$

Once the former operator is obtained, a simulation of a HIL test can be carried out. To simplify the process, the model in contact (which replaces the real pantograph) is a single spring as shown in Fig. A.11. This spring applies a vertical force f_c on the contact point, which is proportional to the difference between the contact point height z_c and a reference value z_0, so that $f_c = k_z(z_c - z_0)$. In this example we use a spring with stiffness $k_z = 10000$ N/m and $z_0 = 5$ mm.

Given a contact force f_c, Eq. (25) provides the contact point height. In the first step of the simulation, the displacement of the contact point is initialised to 0 and the contact force is therefore $f_c(1) = k_z z_0 = 50$ N. By multiplying the first column of $\mathbb{I}(n, \hat{n})$ by this force, we obtain:

$$z_c^1 = 10^{-3} \cdot [1.9022 \ 2.4265 \ 2.3380 \ 1.8791 \ 2.0630 \ 1.9668] \ \text{m}$$

for all $n \in [1, 6]$. In the next step, the displacement of the contact point is $z_c^1(2) = 2.4265 \cdot 10^{-3}$ m and the contact force is $f_c(2) = k_z(z_0 - 2.4265 \cdot 10^{-3}) = 25.7351$ N. This value is used to multiply the second column of $\mathbb{I}(n, \hat{n})$ and the result is added to z_c^1 to compute z_c^2, from which the third value $z_c^2(3) = 3.4803 \cdot 10^{-3}$ can be obtained for the next step.

In the 7-th step, the block number 2 starts and hereinafter, instead of using the force value $f_c(7)$, we use the increment respect to the force on the former block, $f_c(7) - f_c(1)$, to multiply the first column of $\mathbb{I}(n, \hat{n})$. Following this procedure, the contact force obtained is shown in Fig. A.14. The contact force is finally repeated in every block as seen in the figure since the steady-state

39

regime has been achieved. This periodic contact force is:

$$f_c = [14.1319 \quad 14.2372 \quad 14.4190 \quad 14.1001 \quad 14.2078 \quad 14.4236] \text{ N}$$
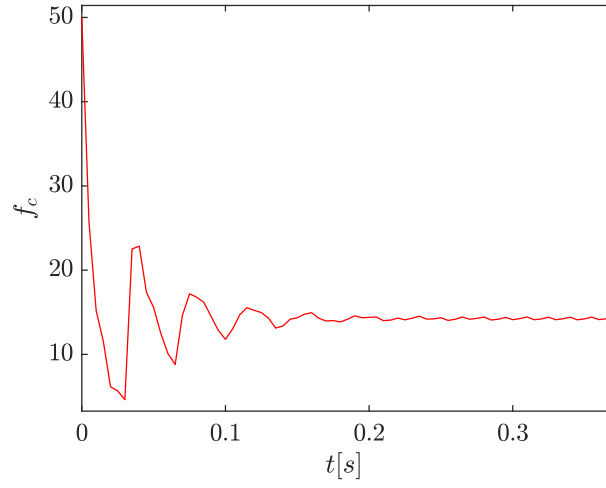
Figure A.14: *Contact force in a simulated HIL test with the academic model.*